J Mater Sci (2009) 44:786–793
DOI 10.1007/s10853-008-3133-9

Enhanced corrosion resistance of discontinuous anodic film on in situ TiB_{2p}/A356 composite by cerium electrolysis treatment

Huanhuan Sun · Xianfeng Li · Dong Chen · Haowei Wang

Received: 23 August 2008 / Accepted: 24 November 2008 / Published online: 27 December 2008

Abstract The agglomerates of TiB_2 particulates and Si phases badly break the continuity of anodized film of in situ TiB_{2p}/A356 composite, which will restrict the improvement of corrosion resistance. In this study, cerium conversion coatings were successfully deposited on anodized TiB_{2p}/A356 composite by electrolysis treatment. Scanning electron microscope observations show that the conversion coatings effectively cover the whole surface of anodized composite. The conversion coatings on continuous porous anodic film are composed of many spherical nano-particulates; however, at the regions without anodic film the conversion coatings present a planar structure. The different morphologies are attributed to the different formation characteristics of cerium conversion coatings at different regions of anodized composite. X-ray photoelectron spectroscopy analysis indicates that the conversion coatings consist of CeO_2, Ce_2O_3, $Ce(OH)_4$, and $Ce(OH)_3$. The potentiodynamic polarization results testify that the integrated surface coatings of anodic film and cerium conversion coating provide a higher degree of protection for in situ TiB_{2p}/A356 composite in a chloride-containing environment.

Introduction

In situ TiB_{2p}/A356 composite has successfully been fabricated by a mixed salt reaction via K_2TiF_6 and KBF_4 technique [1, 2]. TiB_2 particulates are endogenously formed in the composites, which leads to many advantages, such as fine reinforcements [3, 4], having good bonding with the matrix and cleaner reinforcement/matrix interface [5]. Moreover, some researchers have reported that the aluminum metal matrix composites (Al MMCs) reinforced with in situ TiB_2 particulates have many excellent mechanical properties [1, 2, 6–9], such as high strength, high Young modulus. As a new material, in situ TiB_{2p}/A356 composite has also been concerned as a great potential material for industrial applications [1, 2, 6].

Nevertheless, in many instances low corrosion resistant properties [10] and inadequate surface hardness have greatly confined the effective applications of in situ TiB_{2p}/A356 composite. Therefore the fabrication of hard and corrosion resistant coatings on the composite is of great importance.

It is well known that anodizing is a suitable method to improve the surface of aluminum and aluminum alloy with high corrosion resistance and high hardness layer. In recent years, anodization treatment is also attempted to be applied to some Al MMCs. Regrettably, anodic films obtained on the composites either have non-uniform thickness or discontinuous and have many defects (pores and microcracks) [11, 12] due to the hindrance of the reinforcements to the film growth. Thus, in some aggressive circumstances the protection of a single anodic film for Al MMCs is not enough. In order to further enhance the protective properties of anodized films, it will be of great significance to remedy the poor anodic film by appropriate post-treatment. Although some techniques have been well developed for sealing porous anodic films of aluminum and aluminum alloys [13–15], the effective methods to seal anodized Al MMCs are relatively limited. Worthy to be considered was the work by Yu et al. [16], and they prepared cerium conversion coatings to seal the porous film of anodized

H. Sun · X. Li · D. Chen · H. Wang (✉)
State Key Lab of Metal Matrix Composites, Shanghai Jiao Tong University, 800 Dongchuan Road, Shanghai 200240, China
e-mail: hwwang@sjtu.edu.cn

SiC_p/Al6061 composite by a spontaneous chemical reaction in a water-based solution containing $Ce(NO)_3$ and H_2O_2. Moreover, the corrosion test indicated that the cerium sealed coatings could afford higher corrosion resistance for SiC_p/Al6061 composite. Introducing rare-earth element conversion coating to seal anodic film will be a promising method because rare-earth salts are environmentally friendly and relatively cheap. But if a chemical conversion treatment is employed to seal the anodized film, a long time will be required for a highly protective coating to be obtained.

The electrolysis deposition is an attractive technique for the preparation of thin film since it offers several advantages, such as short treatment time, low processing temperature, and controlled the thickness of the film [17]. In this study, cerium electrolysis treatment was successfully used to fabricate a layer of cerium conversion coatings on the surface of discontinuous anodic film of in situ TiB_{2p}/A356 composite. The characteristics of the cerium conversion coatings were studied by scanning electron microscope (SEM), energy dispersive spectroscopy (EDS), and X-ray photoelectron spectroscopy (XPS), and possible formation process of the conversion coatings was proposed. The protection degree of the coatings was evaluated by measuring the potentiodynamic polarization curves in 3.5 wt.% NaCl solution.

Experimental

In situ 15 wt.% TiB_{2p}/A356 (7.0% Si, 0.35% Mg, Al remainder) composite ingot was fabricated with an exothermic reaction process via K_2TiF_6 and KBF_4 salts. The detailed description of the fabrication method could be found elsewhere [1]. The composite ingot was submitted to T6 which included solution treatment at 550 °C for 10 h, water quenching at 70 °C and aging treatment at 150 °C for 8 h for the subsequent use. XRD analysis confirmed that the main phases of the composite were α-Al, TiB_2, and Si.

The 30 mm × 30 mm × 6 mm samples were cut from the composite ingot. They were polished with 1000# abrasive paper, rinsed with acetone, then with tap water, and surface-activated using 1:1 HNO_3 for 30 s at room temperature. Prior to anodizing, the samples were fully rinsed with distilled water. Anodizing was conducted in the stirred solution with 16.0 wt.% sulfuric acid and 1.0 wt.% oxalic acid mixed electrolytes at a current density of 0.01 A/cm^2 and at 15 °C for 45 min and Pb sheet served as the cathode. After anodizing, the samples were thoroughly washed with distilled water. Subsequently, electrolysis treatment was performed in the stirred solution containing 0.6–0.7 g/L $CeCl_3$ and 3.0 g/L H_2O_2 (30%) at a constant voltage of 3 V for 45 min at room temperature. During this process, the anodized composites served as cathode and Pb sheet was the anode. After electrolysis treatment, the coating samples were rinsed with distilled water and dried with air.

The surface structures of the composite before and after anodizing as well as the morphologies of cerium conversion coatings were examined by SIRION-200 Field Emission SEM. The compositions of the conversion coatings and the valence states of the elements were investigated with EDS and XPS (PHI-5300/ESCA) with monochromatic Al Kα radiation.

The corrosion resistance of coated composites was estimated in a 3.5 wt.% NaCl solution by potentiodynamic polarization test on a CHI660C electrochemical workstation. A saturated calomel reference electrode and a Pt counter electrode were used. The polarization scans were started at a rate of 1 mV/s once the samples reached a steady open circuit potential in the test solution.

Results and discussion

Morphologies of the composite before and after anodizing

Figure 1a shows the microstructure of 15 wt.% TiB_{2p}/A356 composite before anodizing. It is noticed that many agglomerates occupy the sites between α-Al dendrites. The microstructure is in agreement with the observation of Kumar's report, and the agglomerates are composed of fine and aggregated TiB_2 particulates and Si phases [18]. Figure 1b gives the surface morphology of anodized composite. It is apparent that the anodic film is discontinuous. When comparing with Fig. 1a, it could be confirmed that the agglomerates badly disable the formation of anodic film and break the continuity of the anodized film. Also, some pores and micro-cracks are found on the surface of anodized composite, which will limit the improvement of corrosion resistant properties of composite surface.

Characteristics of cerium conversion coating deposited on anodized composite

Cerium electrolysis treatment was employed to remedy the defective anodic film in this study, in order to obtain an integrated protection coating on the surface of in situ TiB_{2p}/A356 composite.

Microstructure of cerium conversion coating

SEM observations find that cerium conversion coatings have been successfully deposited on the whole surface of

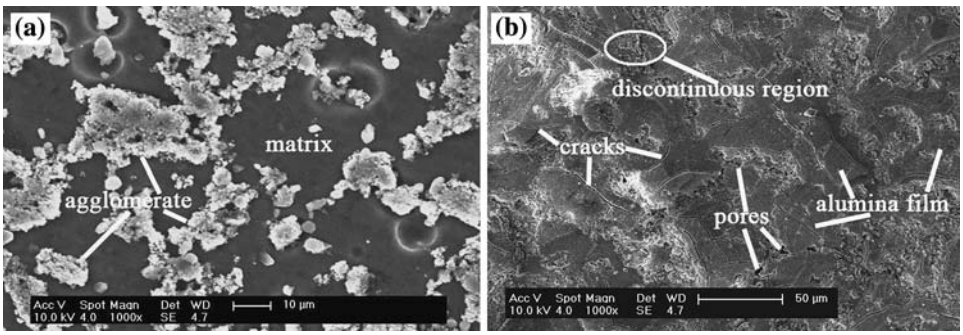

Fig. 1 SEM images of in situ TiB_{2p}/A356 composite before (**a**) and after (**b**) anodizing

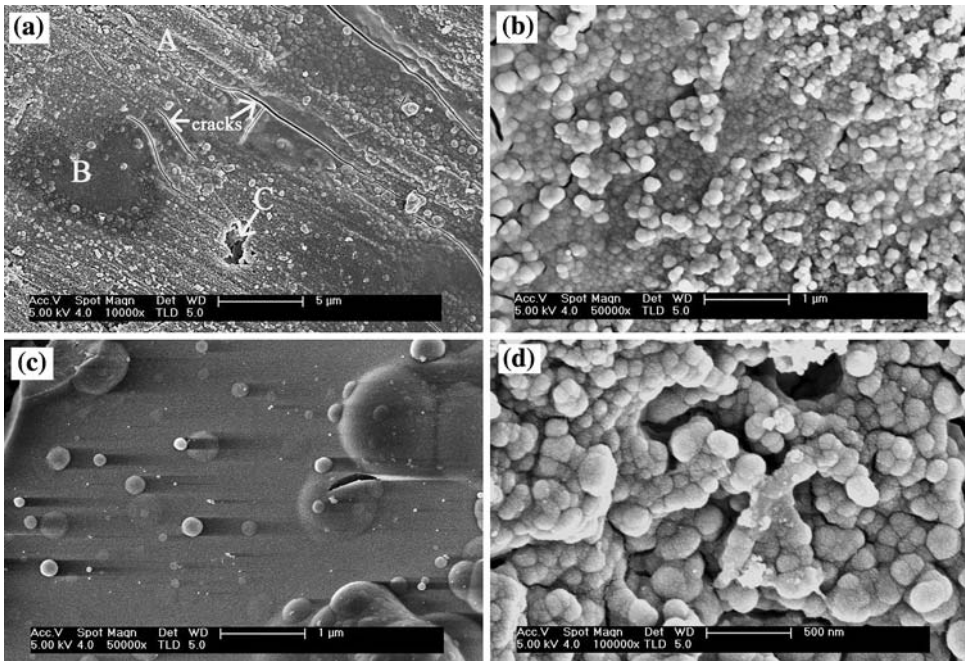

Fig. 2 Surface morphologies of cerium conversion coatings on anodized TiB_{2p}/A356 composite. **a** The whole morphology. **b** Higher magnification view of the light-colored region "A" observed in (**a**). **c** Higher magnification view of the dark-colored region "B" observed in (**a**). **d** Higher magnification view of the region "C" observed in (**a**)

anodized composite, as shown in Fig. 2a. But the thickness of the conversion coatings cannot be exactly measured because the anodized composite underneath the conversion coatings is uneven. Noticeably, the coatings also effectively cover most pores and micro-cracks of the original anodized composite. The conversion coatings exhibit two types of colored regions and they are marked as light-colored region "A" and dark-colored region "B." Figure 2b and c shows the magnification images of "A" and "B," respectively. It can be seen that the conversion coatings at region "A" are composed of many spherical particulates, and the size of the particulates is about 100 nm. While the region "B" shows a completely different morphology, namely a planar coating. A little amount of spherical particles can also be observed on the planar coatings, and the biggest size of individual deposit is up to 1 μm. EDS studies show that the composition of the region "A" is (in wt.%) 55.51 Al, 26.56 O, 7.42 Ce, 1.08 Ti, 13.6 Si, 0.43 Mg, and 7.64 S, and the composition of the region "B" is (in wt.%) 16.00 Al, 14.31 O, 43.78 Ce, 15.83 Ti, 6.49 Si, 0.05 Mg, and 3.53 S. When comparing with the EDS results acquired from regions "A" and "B," higher Ti and Si signals from the region "B" imply that the dark-colored region is corresponding to the conversion coatings formed on the discontinuous region of anodized film, whereas light-colored region "A" is corresponding to the cerium conversion coatings deposited on continuous anodic film. Moreover, the amount of element Ce is much higher at region "B" than at region "A," which indicates that the conversion coatings are much easier to deposit and grow at the regions without anodic film than on the continuous anodic film. Simultaneously, a few fine cracks are found at the dark-colored coatings or at their surroundings, and the formation of the cracks may be attributed to the dehydration of the high thickness coatings at these regions after dried treatment. At location "C" in Fig. 2a, a relatively larger cavity is found. Magnified observation testifies that spherical particulates are effectively deposited in the cavity, as shown in Fig. 2d. Additionally, it must be pointed out that element S in EDS results is from the

sulfuric acid electrolytes for anodizing. It can be deduced that the different colors of the conversion coatings are mainly due to different coating morphologies at different regions. Also, it may be associated with the scraggly surface of anodized composite as well as non-uniform thickness of the conversion coatings, which also result in the different images under SEM.

XPS studies of cerium conversion coating

In order to further analyze the compositions and chemical states of the elements in the cerium conversion coatings, XPS was performed to study the coatings. Figure 3a shows the XPS survey spectrum obtained from cerium conversion coatings on anodized composite. The peaks in the survey spectrum indicate that the main elements in the conversion coatings are Ce and O. The presence of C may be due to the accumulation of contaminants during exposure to air [19]. The peak of binding energy of Al 2p is 74.3 eV (Fig. 3b), which is consistent with the binding energy of Al 2p orbit of Al_2O_3. So Al and a small amount of O may be from Al_2O_3 film underneath cerium conversion coatings. Figure 3c and d shows the XPS high-resolution spectra of Ce 3d and O 1s, respectively. Ce 3d spectrum shows eight components with binding energies. The binding energy peaks appear at 897.7 and 916.1 eV, which are the characteristics of Ce^{4+} compounds such as CeO_2 and $Ce(OH)_4$ [20]. The binding energy peaks at 884.6 and 904.6 eV are associated with Ce^{3+} compounds such as Ce_2O_3 and $Ce(OH)_3$ [21]. Concerning the O 1s region, it has two obvious binding energy peaks. One is corresponding to oxygen in the form of Ce–O group (529.2 eV) and the other is centered at 531.4 eV, which is corresponding to oxygen from Al_2O_3 film (531.0 eV) and oxygen in the form of Ce–OH group (531.6 eV) [22]. So it is concluded that the conversion coatings are mainly composed of CeO_2, Ce_2O_3, $Ce(OH)_4$, and $Ce(OH)_3$.

Possible formation process of cerium conversion coating

The formation mechanism of cerium conversion coatings is highly complicated, which is associated with many factors, such as fabrication methods, processing parameters, submitted materials, and so on. According to above experimental results, the possible formation process of cerium conversion coatings during electrolysis treatment was proposed.

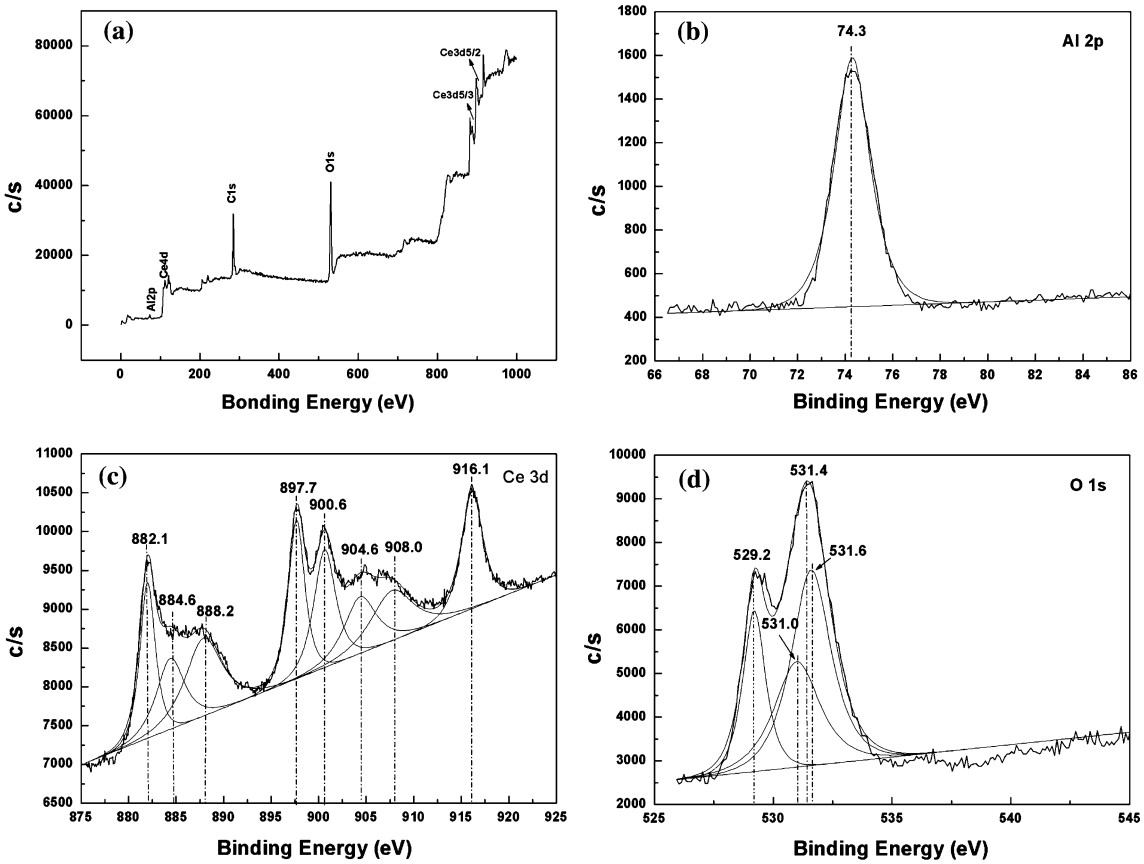

Fig. 3 XPS spectra of cerium conversion coatings on anodized composite. **a** Survey spectrum. **b** Al 2p spectrum. **c** Ce 3d spectrum. **d** O 1s spectrum

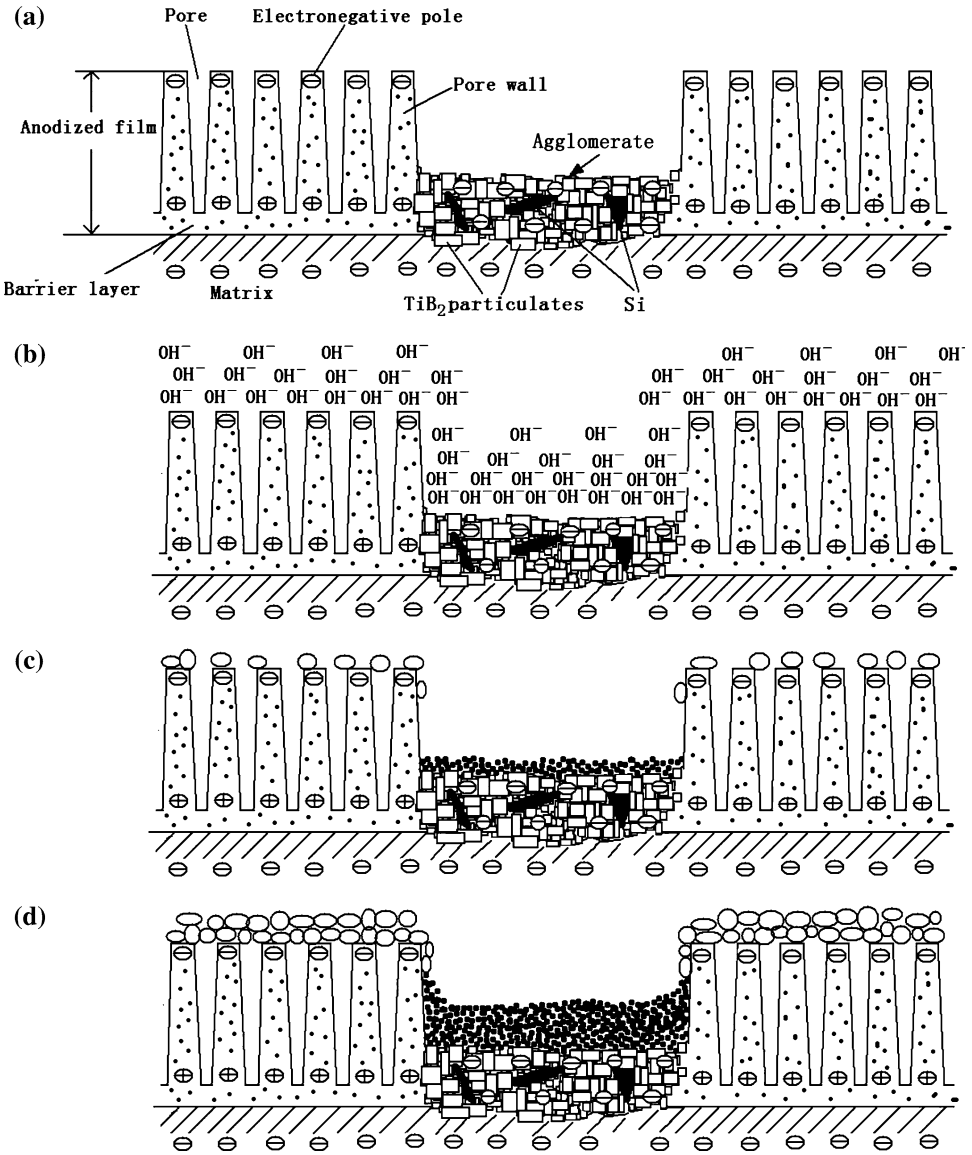

Fig. 4 Schematic diagrams showing formation process of cerium conversion coatings on anodized composite during electrolysis treatment. **a** Polarized anodized composite. **b** High concentration gradient of OH^- near the anodized composite. **c** Formation of cerium compound particulates. **d** Cerium conversion coating on anodized composite

A schematic illustration of the whole anodized film on 15 wt.% TiB_{2p}/A356 composite is depicted in Fig. 4a, and the surface layer of anodized composite is primarily consisted of the continuous porous alumina film and the agglomerates of TiB_2 particulates and Si phases.

In this study, the cerium salt solution used for electrolysis treatment is yellow, which is attributed to the formation of the hydroxide species $Ce(OH)_2^{2+}$ after addition of H_2O_2 (Eq. 1) [23].

$$2Ce^{3+} + H_2O_2 + 2H_2O \rightarrow 2Ce(OH)_2{}^{2+} + 2H^+. \quad (1)$$

When the anodized TiB_{2p}/A356 composite serves as the cathode, the transmission mechanism of the electron in the surface layer is complex.

For continuous porous anodic film, Bipolar Theory [24] is applied to interpret the formation process of cerium conversion coatings. Alumina film has some characteristics of a semiconductor. When cathodic voltage is forced on anodic film, porous film will be polarized. An inner electric field is formed in anodic film, as shown in Fig. 4a. The bottom of porous layer shows electropositivity, whereas the top of pore wall of porous layer has negative charges. Thus, electrochemical reduction reaction of H_2O_2 will easily occur on the top of pore wall.

$$H_2O_2 + 2e \rightarrow 2OH^-. \quad (2)$$

Nevertheless, the bigger agglomerates of TiB_2 and Si badly disrupt the anodic film. During electrolysis treatment, they are directly exposed in cerium salt solution. It is known that TiB_2 has relatively better conductivity (electrical resistivity $\rho \approx 15 \times 10^{-6}\ \Omega$ cm). The conductivity of Si is poor (electrical resistivity $\rho > 0.1$–$1000\ \Omega$ cm), however, it is aggregated together with a large amount of TiB_2 particulates. When forced on a cathodic

voltage, the agglomerates with many TiB_2 particulates will show very strong negative electric property because they connect with the polarized aluminum matrix, and the above-mentioned reduce reaction (Eq. 2) will more drastically occur on these cathodic sites.

As a result, the increase in OH^- results in the increase in the pH value of the cerium salt solution, and the concentration gradient of OH^- is generated near the anodized composite. Especially, a higher OH^- concentration will be generated near the agglomerates (Fig. 4b). When the pH value of the solution near the anodized composite is up to 8, the electrochemical deposit reaction will proceed [25] on the top of both porous anodic film surface and the exposed agglomerates, according to Eq. 3. Additionally, another deposit reaction may also occur, according to φ–pH plot of the Ce–H_2O system [25] (Eq. 4) if the concentration of OH^- is much higher.

$$Ce(OH)_2{}^{2+} + OH^- + e^- \rightarrow Ce(OH)_3 \rightarrow \frac{1}{2}Ce_2O_3 + \frac{3}{2}H_2O, \quad (3)$$

$$Ce(OH)_2{}^{2+} + 2OH^- \rightarrow Ce(OH)_4 \rightarrow CeO_2 + 2H_2O. \quad (4)$$

The higher OH^- concentration near the exposed agglomerates is in favor of chemical reaction processes of Eqs. 3 and 4, and it promotes the rapid nucleation of the countless and finer cerium compounds. And the result is that these cerium compound particulates tightly deposit together and form a planar coating, as shown in Fig. 4c. Johnson et al. [26] reported that the particulates in the cerium oxide conversion coatings were <10 nm, and these particulates could be observed by using the transmission electron microscopy. Reversely, on continuous porous alumina film, the nucleation of the cerium compounds is lower and the size of the compounds is bigger, due to lower OH^- concentration around it. It must be pointed out that the dissolution of porous alumina film will occur, as shown in Eq. 5. But the deposition rate of the conversion coatings will exceed the dissolution rate of anodic film with increasing the electrolysis time [27]. The result is that porous alumina film is gradually sealed.

$$Al_2O_3 + 2OH^- \rightarrow 2AlO_2{}^- + H_2O. \quad (5)$$

The precursor cerium compound nuclei may act as sites for further deposition. New deposits are continuously added onto them, which results in a coating thickness growth (Fig. 4d). Based on the above analysis, it is reasonable to deduce that the conversion coatings on exposed agglomerates are much thicker than those on the continuous alumina film, which is also testified by the results of EDS analysis. Simultaneously, with the agglomerates are gradually covered, a little amount of bigger cerium compounds are also generated on the planer coatings, as shown in Fig. 2c, due to the decrease in the nucleation rate.

Certainly, the pores, micro-cracks as well as big cavities on the anodized composite will also generate a certain effect on the formation process of the cerium conversion coatings. The reason is that these defective sites often supply a high energy density, which will facilitate the nucleation and growth of deposits [28]. Further detailed studies about the deposition of the cerium compounds on the defects are needed to confirm this hypothesis.

Potentiodynamic polarization analysis

In order to evaluate the protectiveness of the coatings for the composite, the electrochemical potentiodynamic polarization technique was employed in this study.

The typical polarization curves in 3.5 wt.% NaCl solution of bare composite and anodized composites with and without conversion coatings are shown in Fig. 5. The corrosion current density values of all the tested samples are obtained by the Tafel extrapolation method [29]. The results show that the bare composite has a highest current density (4.868×10^{-5} A/cm^2), and its corrosion current density rapidly increases with increasing potential above the corrosion potential (−0.765 V). These indicate that the bare composite is easily corroded in NaCl solution. After anodizing, corrosion starts at a relatively lower current density (2.301×10^{-6} A/cm^2) and a slightly more positive corrosion potential (−0.723) than the bare composite. Moreover, the corrosion current density increases with the potential less markedly, indicating that the corrosion is restrained after anodizing to a certain extent. When the anodized composite is covered a layer of cerium conversion coatings after electrolysis treatment, and the corrosion potential of anodized composite with conversion coatings remains almost at the same level as that of the anodized

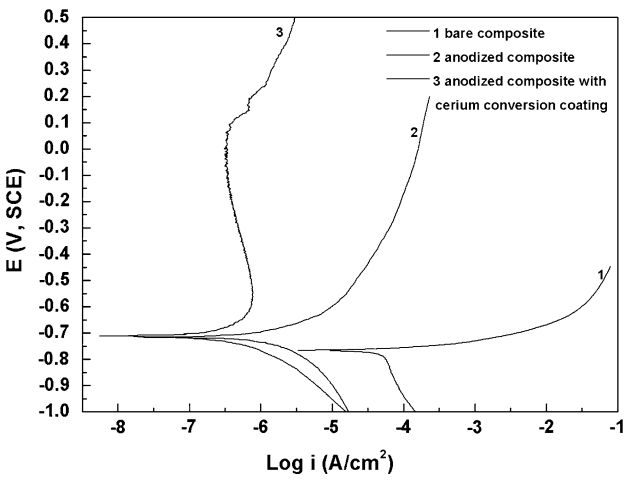

Fig. 5 Potentiodynamic polarization curves for bare composite and anodized composites with and without cerium conversion coatings in 3.5 wt.% NaCl solution

composite without conversion coatings. The corrosion current density (5.957×10^{-7} A/cm^2) of anodized composite with cerium conversion coatings further decreases compared with that of anodized composite without conversion coatings, and it is approximately two orders of magnitude lower than that of bare composite. Meanwhile, a classical well-defined passive region is observed, and a large difference value of $E_{pit} - E_{corr}$ (about 0.7 V) was found, indicating that the pitting has been greatly delayed by anodic film with cerium conversion coatings.

For the bare composite, the agglomerates of TiB_2 and Si exposed on the composite surface may break nature film and weaken the protection of surface film for the composite matrix. Thus, aluminum of the composite surface undergoes active dissolution in chloride ion solution during polarization. After anodizing, alumina film which prevents the composite matrix from being in contact with the solution. Nonetheless, the pores and micro-cracks on anodized composite provide the paths for the corrosive solution [30]. Moreover, these defects (pores and micro-cracks) are the favorable sites where the corrosion intermediates are absorbed and concentrated [30, 31]. The corrosion intermediates can transfer through the defective film and reach the bottom of anodic coating, which leads to the increase in polarization current. When the polarization current reaches a certain value, the corrosive intermediate will react with the composite matrix under the anodic film. After cerium electrolysis treatment, the whole surface of anodized composite is covered by cerium conversion coatings successfully, and most defects are effectively sealed. Cerium conversion coatings can provide a certain protection for composite matrix. Especially, the synergistic effect of anodized film and conversion coatings is to hold back the transfer of the corrosive intermediates to a greater extent, so the corrosion current drastically decreases and the corrosion process is slowed down. During polarization corrosion, there are no current increases at a larger potential that can be related to high pitting resistance of the anodized composite with cerium conversion coatings. These polarization results testify that integrated protection coatings afford more effective protections for the composite than the single and the defective anodized film, and that the treatment method for in situ TiB_{2p}/A356 composite is feasible.

Conclusion

Cerium conversion coatings were successfully fabricated on the whole anodized TiB_{2p}/A356 composite by electrolysis treatment method. SEM observations find that the conversion coatings exhibit two types of colored regions, namely light-colored region and dark-colored region. At light-colored region, the conversion coatings are composed of many spherical nano-particulates. At dark-colored region, the conversion coatings present a planar structure. The results of EDS analysis testify that light-colored coatings formed on continuous porous anodic film, and formation mechanism of conversion coatings can be interpreted by Bipolar Theory. The dark-colored planar coatings form on the region without anodic film, and the formation mechanism of conversion coatings is attributed to the good conductivity of TiB_2 particulates in the exposed agglomerates. The main compositions of the conversion coatings are CeO_2, Ce_2O_3, $Ce(OH)_4$, and $Ce(OH)_3$. The integrated protection coatings consisted of anodic film and cerium conversion coatings could effectively hold back corrosive intermediates and protect the composite matrix, allowing a higher protection degree for in situ TiB_{2p}/A356 composite.

References

1. Yi HZ, Ma NH, Li XF, Zhang YJ, Wang HW (2006) Mater Sci Eng A 419:12
2. Mandal A, Chakraborty M, Murty BS (2008) Mater Sci Eng A 489:220
3. Lakshmi S, Lu L, Gupta M (1998) J Mater Process Technol 73:160
4. Zhang YJ, Ma NH, Wang HW, Le YK, Li SC (2005) Scr Mater 53:1171
5. Lu L, Lai MO, Chen FL (1997) Acta Mater 45:4297
6. Yi HZ, Ma NH, Zhang YJ, Li XF, Wang HW (2006) Scr Mater 54:1093
7. Tee KL, Lü L, Lai MO (2003) Mater Sci Eng A 339:227
8. Kennedy AR, Karantzalis AE, Wyatt AM (1999) J Mater Sci 34:933. doi:10.1023/A:1004519306186
9. Ceng L, Zhang J (2001) J Mater Sci Technol 17:675
10. Sekhawat DS, Chakraborty M, Chatterjee UK (2005) Mater Sci Forum 475–479:449
11. Shahid M (1997) J Mater Sci 32:3775. doi:10.1023/A:1018623623116
12. Picas JA, Forn A, Rupérez E, Baile MT, Martín E (2007) Plasma Process Polym 4:S579
13. Cheng BR, Hao L (2000) Met Finish 98(5):48
14. Snogan F, Blanc C, Mankowski G, Pébère N (2002) Surf Coat Technol 154(1):94
15. Zuo Y, Zhao PH, Zhao JM (2003) Surf Coat Technol 166:237
16. Yu X, Cao C, Yao Z (2000) Mater Sci Lett 19:1907
17. Creus J, Brezault F, Rebere C, Gadouleau M (2006) Surf Coat Technol 200:4636
18. Kumar S, Subramanya Sarma V, Murty BS (2008) Mater Sci Eng A 476:333
19. Shyu JZ, Otto K, Watkins WLH, Graham GW, Belitz RK, Gandhi HS (1988) J Catal 114:23
20. Yu XW, Li GQ (2004) J Alloys Compd 364:193
21. Pardo A, Merino MC, Arrabal R, Viejo F, Muñoz JA (2007) Appl Surf Sci 253:3334
22. Arnott DR, Ryan NE, Hinton BRW, Sexton BA, Hughes AE (1985) Appl Surf Sci 22–23:236
23. Aldykiewicz AJ, Davenport AJ, Isaacs HS (1996) J Electrochem Soc 143:147

24. Gao YZ (1985) Surface treatment of aluminum alloys. Metallurgy Industry Press, Beijing (in Chinese)
25. Davenport AJ, Isaacs HS, Kendig MW (1991) Corros Sci 32:653
26. Johnson BY, Edington J, O'Keefe MJ (2003) Mater Sci Eng A 361:225
27. Li GQ, Li D, Li JQ, Guo BL, Peng MX (2001) J Chin Soc Corros Prot 21:150 (in Chinese)
28. Li FB, Newman RC, Thompson GE (1997) Electrochim Acta 42:2455
29. Jone DA (1992) In: Johnstone D (ed) Principles and prevention of corrosion. Macmillan, New York
30. Duan HP, Du KQ, Yan CW, Wang FH (2006) Electrochim Acta 51:2898
31. Guo HF, An MZ (2005) Appl Surf Sci 246:229